Received: 7 May 2017 | Revised: 7 June 2017 | Accepted: 15 June 2017

DOI: 10.1002/jat.3507

Journal of Applied Toxicology

RESEARCH ARTICLE

In vitro evaluation of the internalization and toxicological profile of silica nanoparticles and submicroparticles for the design of dermal drug delivery strategies

Sara Vicente[1] | Claudia Moia[2] | Huijun Zhu[2] | Xavier Vigé[1]

[1] SANOFI Research & Development, Translational Sciences Unit, 91385 Chilly-Mazarin, France

[2] Environmental Science and Technology Department, School of Applied Sciences, Cranfield University, Bedford MK43 0AL, UK

Correspondence
Sara Vicente, PhD, Institute for Bioengineering of Catalonia (IBEC), C. Baldiri Reixac 10-12, 08028 Barcelona, Spain.
Email: svicenteo@ibecbarcelona.eu

Funding information
FP7 People: Marie-Curie Actions, Grant/Award Number: HPMI-CT-2001-00110 and MCITN-2011-289554

Abstract

The use of colloidal silica nanoparticles and sub-microparticles (SiPs) have been considered a very interesting strategy for drug delivery applications. In the present study, we have focused our attention on the suitability of these nanomaterials as potential carriers for dermal drug delivery, thus studying their toxicological profile *in vitro*, cellular uptake and intracellular localization in both human keratinocytes (K17) and human dermal fibroblasts (HDF) as a function of their particle size (SiPs of 20, 70, 200 and 500 nm). Full characterization of these aspects enabled us to observe a strong cell-type dependency in terms of cytotoxicity and cell internalization, whereas particle size was only relevant for ultra-small SiPs (20 nm), being the most toxic SiPs. For 70, 200 and 500 nm SiPs, the differences in uptake and intracellular trafficking determined the different toxicological profiles in K17 and HDF. In addition, these characteristics can further define different drug delivery strategies. Hence, phagocytosis has been identified as the main internalization mechanism for K17, and caveolae-mediated endocytosis for HDF. This relevant information led us to conclude that fibroblasts would be optimal targets for delivering delicate therapeutic molecules such as proteins or genetic material using SiPs while maintaining a low toxicity profile, whereas keratinocytes could enable accelerated drug release therapies based on SiPs.

KEYWORDS

amorphous silica nanoparticles, internalization, intracellular trafficking, nanotoxicology, skin delivery

1 | INTRODUCTION

The application of nanotechnology in medicine has been increasingly gaining attention and recently undergoing intensive development in different scientific fields (Duncan & Gaspar, 2011). Indeed, the great development of new nanotechnological tools have been applied in a variety of biomedical areas such as drug delivery (Alex & Sharma, 2013; Correia-Pinto, Csaba, & Alonso, 2013; Krishnamurty, Ke, & Yang, 2015; Ponnappan & Chugh, 2015), imaging (Bakhtiary et al., 2016), and more recently theranostics (Muthu, Leong, Mei, & Feng, 2014). The result of this vast research is the increasing number of new medicines based on nanotechnologies undergoing clinical trials (Caster, Pate, Zhang, & Wang, 2017). However, the use of nanomedicines has also become the subject of debate regarding its safety for their application in humans, especially from a regulatory point of view (Duncan & Gaspar, 2011). As a consequence, measuring their toxicological impact, both *in vitro* and *in vivo*, has become a fundamental step in the first phases of pre-clinical studies of new nanomedicines to ensure their safety and to proceed to further clinical development (Arora, Rajwade, & Paknikar, 2012; Santamaria, 2012).

Amorphous silica is one of the most abundant synthetic materials produced every year. It has been used as an additive in multiple different products such as cosmetics, drugs, varnishes, and food (Fruitjier-Pölloth, 2012). As a nanosized material, in the last few years, it has been attracting interest for several biomedical applications (cancer therapy, DNA transfection, drug delivery) due to its biocompatibility, low toxicity and scalable synthetic availability (Kettiger, Karaman, Schiesser, Rosenholm, & Höwyler, 2015). In addition, the versatility of this nanomaterial is one of its most attractive features. Particle size, porosity and shape can be finely tuned for diverse applications (Napierska, Thomassen, Lison, Martens, & Hoet, 2010); its surface can also be easily modified to achieve specific drug or chemical loading, as well as site-specific targeting (Liberman, Mendez, Trogler, & Kummel, 2014). The possibility to combine these properties,

together with a well-documented tolerance by different cell types (Kettiger et al., 2015), makes nanosized silica particles a desirable platform for biomedical applications.

Due to these promising characteristics, the potential use of silica particles for transdermal delivery and controlled release of drugs to the skin has been already proposed (Nafisi, Schäfer-Korting, & Maibach, 2015), although greater attention has been paid to their capacity to permeate through the skin barrier (Iannuccelli et al., 2014; Ugazio et al., 2016). Their low toxic effects on skin cells (Yu et al., 2009) has been already studied due to the hazard concerns of these materials. Therefore, the biological evaluation performed in the present study intends to go further and provide systematic and useful information in terms of biological interaction with target cells (keratinocytes and fibroblasts) to develop a quality-by-design approach based on these interesting materials with the aim of improving the treatment of skin diseases such as fibrosis, psoriasis, melanoma, etc. Some of these diseases have an important genetic component or intracellular target, thus, studying the cellular uptake and subsequent intracellular route also becomes a very relevant issue in these very initial phases of development. As well, proving the safety of amorphous silica of different diameters with the target cells will importantly contribute to a quality-by-design drug delivery system based on silica particles. In summary, in this study, we investigated the *in vitro* toxicity and cellular uptake of amorphous silica particles (SiPs), in particular, silica nanoparticles (SiNP: size <200 nm) and submicroparticles (SMP: size ≥200 nm) as potential drug delivery carriers for dermal applications. SiPs of different sizes were sourced from commercial suppliers without further treatment. The toxicity of these SiPs was assessed using two different types of human skin cells: K17 keratinocytes (K17) and human dermal fibroblasts (HDF), via multi-assays to delineate the mechanisms of cell-type, particle size- and concentration-dependent toxicity. In addition, confocal scanning microscopy was used to study their penetration capacity as well as their intracellular trafficking route.

2 | METHODS

2.1 | Materials: Particles, chemicals and antibodies

LUDOX® amorphous non-porous silica nanoparticles (SiNP20) were purchased from Sigma-Aldrich (Saint Louis, Missouri, USA). SiNP70, SMP200 and SMP500 amorphous non-porous silica particles were obtained from Postnova Analytics GmbH (Landsberg am Lech, Germany). A summary of the characteristics provided by the manufacturers is shown in Table 1. Fluorescein-labelled SiNP70, SMP200 and SMP500 with the same characteristics were obtained from the same provider.

TABLE 1 Characteristics of colloidal silica obtained from manufacturer. N/A: Not available

	SiNP20	SiNP70	SMP200	SMP500
Manufacturer	Sigma-Aldrich	Postnova analytics		
Given size (nm)	20	70	200	500
Surface area (m^2/g)	198–258	43	15	6
Polydispersity	N/A	< 0.2	< 0.2	< 0.2

Paraformaldehyde (PFA) 16% aqueous solution was obtained from Alfa-Aesar GmbH (Karlsruhe, Germany). Bovine serum albumin (BSA) and Triton X-100 were purchased from Sigma-Aldrich. Gelatin was obtained from BioRad (Marnes-La-Coquette, France).

ActinRed®, Lysotracker® Red DND-99, propidium iodide and Hoechst 33342 were purchased from Molecular Probes (Life Technologies Corp., Carlsbad, Calfornia, USA).

Anti-Rab7 (D95F2) XP® rabbit mAb, anti-caveolin-1 (D46G3) XP™ rabbit mAb, anti-rabbit and anti-mouse IgG (H + L), F(ab')2 Fragment (Alexa Fluor® 555 Conjugate) were obtained from Cell Signaling Technology (Beverly, Massachusetts, USA). Anti-LAMP1 (H4B4) mouse mAb were from Santa Cruz Biotechnology Inc. (Dallas, Texas, USA).

2.2 | Particle size measurements and stability in culture media

Dynamic light scattering (DLS) was used to determine the particle size distribution and their dispersion pattern in EpiLife® and 106 media diluted at 50 µg/ml. Three measurements were made for each sample using Zetasizer (Malvern, Worcestershire, UK) at 25°C with a 173° detector. Before particle analysis, the DLS profiles of cell culture media were acquired for the presence of background molecule clusters, which could interfere with the samples measurement.

2.3 | Cells and culture conditions

Human dermal fibroblasts (HDF) isolated from adult skin were from Gibco® (Life Technologies Corp.). To culture these cells, Medium 106 supplemented with LSGS 50X (low serum growth supplement) and penicillin/streptomycin 100 UI/ml (all from Gibco®) were used.

K17 keratinocytes (K17) are immortalized cells produced from normal adult keratinocytes kindly donated by Prof. D. Kelsell (Center for Cutaneous Research, Queen Mary University of London, UK). The complete culture medium was prepared using EpiLife® supplemented with HKGS 100X (human keratinocytes growth supplement) and penicillin/streptomycin 100UI/ml (all from Gibco®). Cells were maintained at 37°C in an atmosphere of 5% CO_2.

2.4 | *In vitro* toxicological analysis

K17 keratinocytes were plated in uncoated 96-well plates at 10,000 cells/well, while poly-D-lysine coated wells were used for HDF and cells were plated at 8,000 cells/well. SiPs were diluted in complete culture medium. The concentrations ranged from 10 to 200 µg/ml. SiPs were then incubated with the cells for 24 h.

2.4.1 | WST-1

To evaluate the metabolic activity of the cells, the cell proliferation reagent WST-1 was used (Roche Applied Science; Mannheim, Germany). The quantification of soluble formazan dye produced by metabolically active cells was measured by spectrophotometry at 450 nm. The cell viability rate was calculated by considering the signal of non-treated cells as the 100% viability.

2.4.2 | Propidium iodide staining and cell counting

Propidium iodide (PI) can stain the nucleus of membrane-compromised cells. After 24 h of incubation with SiPs, 5 μg/ml of PI diluted in PBS were added and incubated for 20 min. Non-treated cells and positive controls, consisting of cells incubated with Triton X-100 0.025% for 10 min, were included in the test. After treatment with PI, cells were washed with PBS and fixed using a solution of PFA 4% (in PBS). Then, all the nuclei in the sample were stained with Hoechst 33342 at 0.1 mg/ml for 10 min at room temperature (RT).

For cell counting, a wide field fluorescence microscope (Zeiss Axio Observer Z1, Jena, Germany) was used. Images acquisition and post-acquisition analysis were performed using Morphostrider software (Exploranova, La Rochelle, France). 16 fields (840.4 × 640.3 μm) per well were acquired using an objective 10× and the adequate filter cubes for Hoechst and PI to image a large surface of the well.

In the post-analysis process, both Hoechst- and PI-labelled nuclei were counted, and the ratio of the number of PI-labelled cells versus the number of Hoechst-labelled cells was calculated.

2.4.3 | LDH release

To measure the level of lactate dehydrogenase (LDH) released from damaged cells, the CytoTox 96® Non-Radioactive Cytotoxicity Assay (Promega, Madison, Wisconsin, USA) was used. Non-treated cells and positive controls (Triton X-100 0.025%; 30 min) were also included. After treatment with SiPs for 24 h, the level of LDH in the culture medium of treated cells and controls was measured according to manufacturer's instructions. The levels of LDH of the positive control were considered as 100%.

2.4.4 | Caspase 3/7 activity measurement

To measure the levels of caspase 3/7, the Apo-ONE Homogeneous Caspase-3/7 Assay (Promega) was used. This method allows the quantification of the caspase 3/7 by the transformation of the kit reagent into a fluorescent molecule by these enzymes. The analysis was performed according to the manufacturer's protocol, and the measurement of the fluorescent signal was performed at 485 nm (excitation) and 530 nm (emission). Non-treated cells were used as negative control (non-apoptotic cells).

2.5 | Internalization and intracellular localization of SiPs

K17 keratinocytes were plated in 8-well Ibidi μ-slides (Ibidi, Martinsried, Germany) with ibiTreat surface at 15,000 cells/well. For HDF, poly-D-lysine-coated 8-well ibidi μ-slides were used at 12,000 cells/well.

Fluorescein-labelled SiNP70, SMP200 and SMP500 at 10 μg/ml were incubated for either 2 or 24 h with both cell types. Cells were then washed with PBS, fixed with PFA 4% (15 min, RT) and permeabilized with Triton X-100 0.5% (10 min, RT). Samples were blocked and primary antibodies were incubated overnight at 4°C using adequate dilution. After extensive washing, secondary antibodies at 1:1000 were incubated for 1 h at RT. Cells were then washed with PBS and nuclei stained with Hoechst 33342 at 0.1 mg/ml (10 min, RT).

To stain lysosomes, SiPs were removed and Lysotracker® Red DND-99 diluted in culture medium at 50 nM was added and incubated for 1 h at 37°C. Lysotracker® was replaced with fresh medium. Imaging was performed in living cells.

Images were obtained using a Carl Zeiss Confocal Laser Scanning Microscope (LSM 510; Jena, Germany) in Expert mode Version 4.2 SP1 equipped with Plan-Apochromat 63X/1.4 oil DIC objective. Post-acquisition treatment of images was performed using ImageJ 1.48 (NIH, Bethesda, Maryland, USA).

3 | RESULTS

3.1 | Stability of SiPs in culture media

The hydrodynamic (H_d) size and dispersion properties of SiPs (polydispersion index, PdI), were measured by DLS. As SiPs may behave diversely in different testing media, they were characterized in both EpiLife® and Medium 106, as these media were used for culturing keratinocytes and fibroblasts, respectively. Particle-free media were analysed as background controls for pre-existing clusters of biomolecules such as sugars, amino acids and proteins that might interfere with the measurement of added particles. As shown in Table 2 (for further detailed characterization see the Supplementary Information Figure 1), pre-existing clusters were detected in both nanoparticle-free media. These clusters appeared to be larger in EpiLife® compared to Medium 106, thus reflecting the difference in the composition of each medium.

In EpiLife®, the H_d size of SiNP20, SiNP70 and SMP200 increased in the order of SiNP70 > SiNP20 > SMP200, whereas the H_d size of SMP500 showed little difference from its given size. Particle aggregation and sedimentation were detected for SiNP20 and SiNP70. SMP200 showed an H_d size increment of 1.5-fold compared to its given size, while SMP500 showed a H_d size (530/488) compatible with the one given by the manufacturer and good dispersion (0.2).

In Medium 106, H_d of SiNP20 increased 5.4-folds from its original size, whereas SiNP70 slightly modified its given size (1.4-fold increase). The H_d size of the two SMPs was much smaller than expected with very high PdI, indicating unstable colloidal status. This instability was also confirmed by the formation of solid aggregates for these two SMPs.

This sharp difference in particle behaviour was dependent on the particles and the medium in which they were diluted. As shown in the negative control DLS measurement, the different size average and PdI for both media indicated the presence of different protein clusters, which can play a relevant role in colloidal stability. Furthermore, according to product specifications, the composition and concentrations of salts for each medium was different, which can result in different ionic strength in the media.

3.2 | Cytotoxicity of SiPs

SiNP20, SiNP70, SMP200 and SMP500 have been tested in terms of cytotoxicity using human K17 and HDF cells to assess their impact on cells from different skin layers. For this purpose, different techniques were used to evaluate different toxicological aspects and to

TABLE 2 DLS assay of SiPs diluted in EpiLife® and medium 106 media. Particle free media were analysed as background controls just after mixing the media with the particles (t = 0 h) and after 24 h incubation at 4°C (storage conditions). Results are expressed as average particle size (Ave. [nm]), and polydispersion index (PdI). Data were obtained as intensity. Three measurements were performed for each sample

	Epilife®				Medium 106			
	0 h		24 h		0 h		24 h	
	Ave. (nm)	PdI	Ave. (nm)	PdI	Ave. (nm)	PdI	Ave. (nm)	PdI
NP-free	71 ± 22	0.5	119 ± 20	0.3	17 ± 14	0.4	17 ± 12	0.4
SiNP20	123 ± 74	0.6	130 ± 140	0.9	109 ± 20	0.3	119 ± 27	0.2
SiNP70	1215 ± 525	0.3	3688 ± 3500	1.0	97 ± 20	0.2	100 ± 20	0.2
SMP200	314 ± 80	0.1	362 ± 97	0.2	188 ± 10	0.4	166 ± 20	0.6
SMP500	530 ± 84	0.1	488 ± 83	0.2	87 ± 300	1.0	48 ± 280	1.0

reinforce and validate the results obtained. Initially, the metabolic activity of the cells upon incubation with increasing concentrations of particles was tested using the WST-1 assay. For both cell types, cells incubated with SiNP70, SMP200 and SMP500 in the range of 5 to 200 µg/mL remained viable after 24 h of incubation (80–120%) (Figure 1A, B). The viability levels for SiNP20, on the other hand, indicate a concentration- and cell-dependent cytotoxic effect. In K17, SiNP20 at a concentration > 10 µg/mL led to cytotoxicity levels higher than 80%, while in HDF this threshold increases up to 50 µg/mL.

To confirm cell viability results, double labelling of the nuclei with PI and Hoechst 33342 was performed to verify the number of cells with compromised cellular membrane against a total number of cells. Nuclei counting was then performed and the ratio between PI- and Hoescht-labelled cells was calculated. The results obtained (Figure 1C, D) were

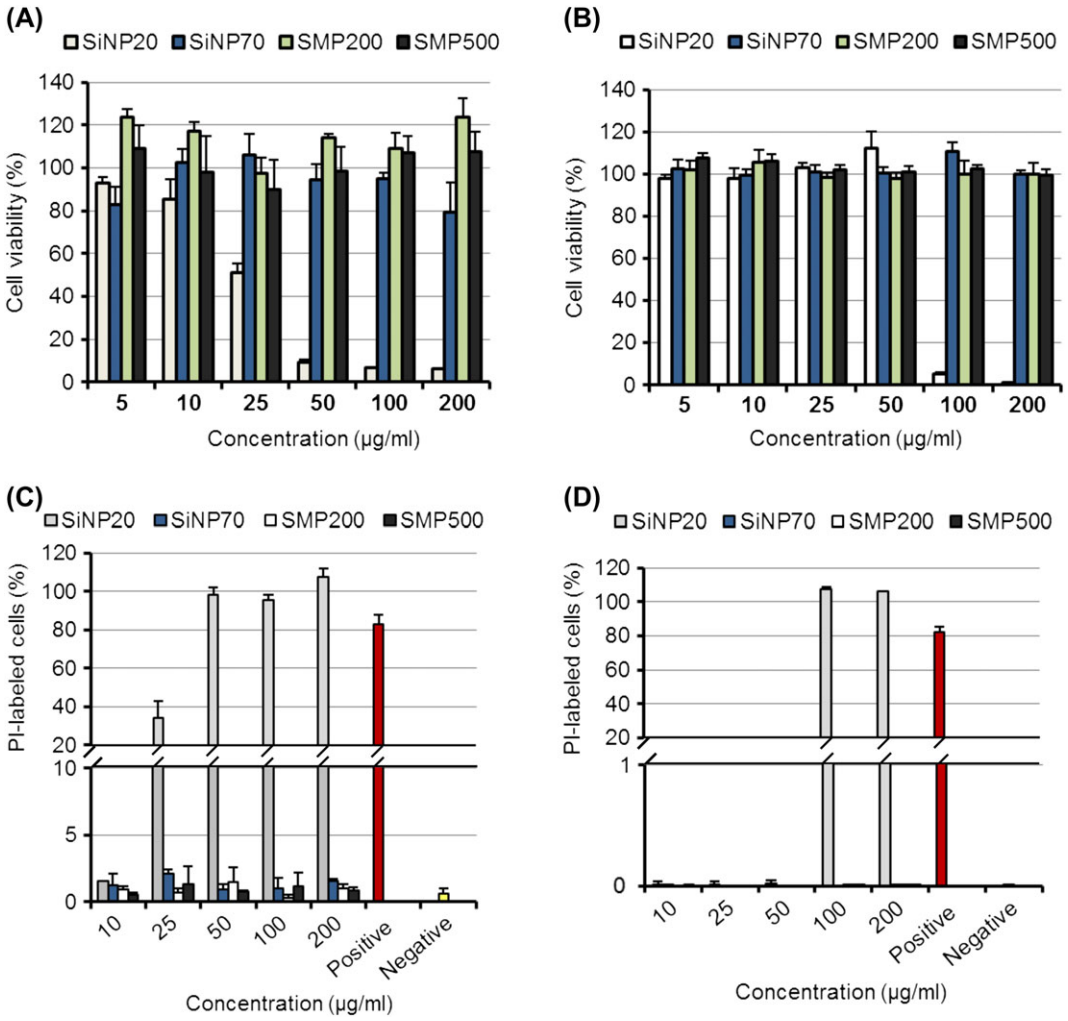

FIGURE 1 Cell viability of keratinocytes (A) and fibroblasts (B) quantified using the WST-1 technique upon 24 h incubation with SiNP20, SiNP70, SMP200 and SMP500. Levels of propidium iodide (PI) labelled keratinocytes (C) and fibroblasts (D) upon 24 h incubation with SiNP20, SiNP70, SMP200 and SMP500. Results are expressed in % of PI-labelled cells regarding the total number of cells in the sample (stained with Hoescht 33342). Results are expressed as % of the untreated cells with average +/− SD of three measurements

consistent with the data obtained by WST-1, as only SiNP20 at concentrations >10 μg/mL for K17, or 50 μg/mL for HDF, resulted in high levels of PI staining. However, the percentage of PI-labelled cells incubated with SiNP70, SMP200 and SMP500 were slightly higher in K17 (around 2%) than in HDF (~ 0%). This difference was somehow inconsistent with the results from the WST-1 assay, in which only a higher variability was detected in K17.

Measuring the extracellular LDH released by damaged cells gave further confirmation on the toxicological characterization of these SiPs. LDH levels released by HDF incubated 24 h with increasing concentrations of particles were consistent with the previous data obtained by WST-1 and PI staining (Figure 2B). However, K17 did not follow the same pattern, as indicated in Figure 2A. In this case, SiNP20 induced LDH levels around 40% for all the concentrations tested (10–200 μg/mL). In addition, a concentration-dependent fate was observed for SiNP70, SMP200 and SMP500, with LDH release near 30% at 200 μg/mL.

Besides SiNP20, no clear induction of cell death was observed for the other types of SiPs despite the long incubation time used. Consequently, we examined if the cells were undergoing any apoptotic process which could not be detected by the above assays. First, the images obtained by microscopy when nuclei were labelled with Hoechst 33342 did not show any abnormal morphology, such as DNA fragmentation. In addition, the activity of caspase 3/7, enzymes that are involved in the initiation of the apoptosis cascade, was quantified. As depicted in Figures 2C & D, an increase of caspase 3/7 activity was detected for SiNP20 at 10 μg/mL in both K17 and HDF (3 and 1.5 fold, respectively). At 100 μg/mL, SiNP20 decreased the caspase activity, which could be due to the high level of cell death, as determined by cell viability assays. For SiNP70, SMP200 and SMP500, no increments of caspase 3/7 activity were observed in HDF either at 10 or 100 μg/mL. However, in K17, the enzyme activity was slightly enhanced up to 1.5 fold increase for SMP200 and SMP500 at 100 μg/mL compared with the control.

3.3 | Internalization and intracellular trafficking of SiPs

The toxicological analysis of SiNP70, SMP200 and SMP500 indicated their low toxicity in both K17 and HDF. This non-toxic behaviour could be due to either low interaction with the cells and consequently low internalization, or to the presence of the nanomaterials intracellularly not directly affecting the normal cell functions. To further test these hypothesises, a microscopy study was performed using fluorescein-labelled SiNP70, SMP200 and SMP500 to study the internalization kinetics in K17 and HDF. Cells were incubated with the different particles at 10 μg/mL at 2 and 24 h and then imaged using laser scanning confocal microscopy (Figures 3A and 4A). For both K17 and HDF, after 2-h incubation, the particles were closely interacting with the surface of the cells and the signal inside the cell was quite low compared with the images acquired at 24 h. These results indicate a progressive uptake in both cell types independently of their particle size.

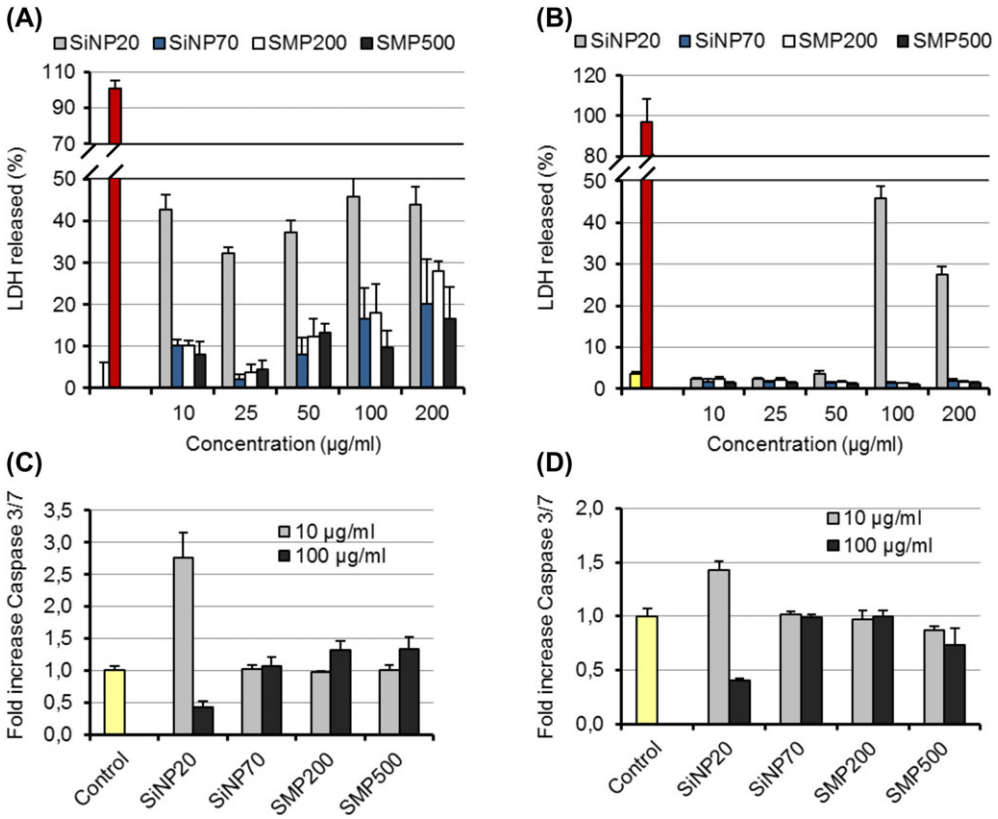

FIGURE 2 LDH release to medium by keratinocytes (A) and fibroblasts (B) upon 24 h incubation with SiNP20, SiNP70, SMP200 and SMP500. Results are expressed in % of LDH in the medium regarding the positive control (100%), as average +/− SD of three measurements. Caspase 3/7 activity induced in keratinocytes (C) and fibroblasts (D) upon 24- h incubation with SiNP20, SiNP70, SMP200 and SMP500. Results are expressed as the fold increase regarding the control (untreated cells) as average +/− SD of three measurements

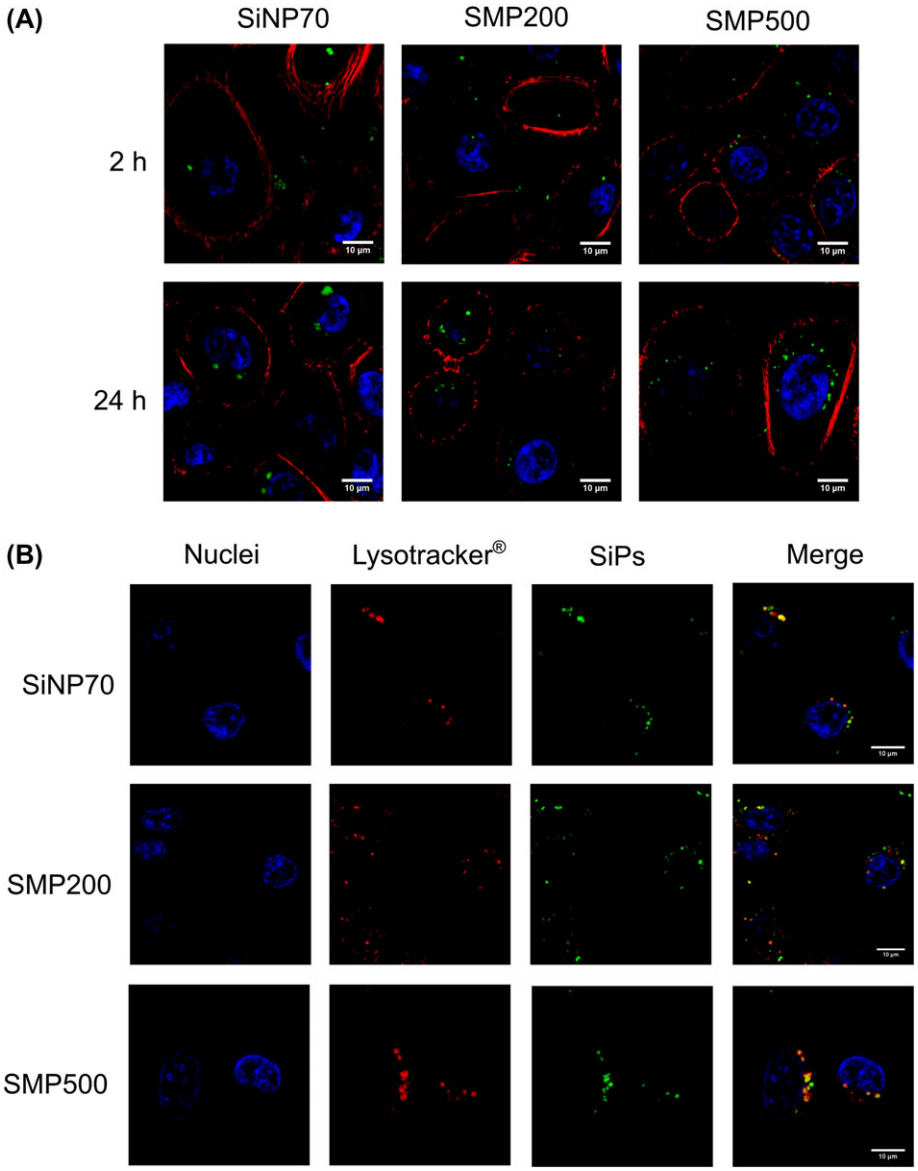

FIGURE 3 LSCM images of keratinocytes incubated with fluorescein-labelled SiNP70, SMP200 and SMP500 at 10 μg/mL. (A) Internalization progress after 2 and 24 h of incubation. Blue channel: Nuclei; green channel: SiPs; red channel: Actin cytoskeleton. (B) Localization of SiPs (green channel) in the lysosomal compartment after 24 h of incubation using Lysotracker® as lysosome marker (red channel). Co-localization of SiPs and Lysotracker® are indicated in yellow/orange colour code, as the result of a combination of green and red channels

Interestingly, a difference regarding particle location in K17 and HDF could be observed after 24 h of incubation. In K17, SiPs were concentrated mostly in a perinuclear region whereas, in HDF, the fluorescent signals were more dispersed in the cytoplasm.

To further study the intracellular location of the particles upon internalization, the lysosomes were labelled using Lysotracker®. The images of K17 (Figure 3B) evidenced a clear co-localization between the fluorescent signal of the particles (green) and the lysosomes (red); whereas in HDF (Figure 4B), these fluorescent signals were located close to each other but not coincident. These observations were equivalent for all the SiPs studied, suggesting that particle size was not a relevant characteristic for the internalization and further intracellular processing. In fact, these two processes seemed to be more related to the cell type and their particular cellular morphology.

Different specific markers of intracellular vesicles were additionally used to further elucidate the intracellular fate of these particles. In fact, Lysotracker® can stain vesicles with intraluminal acidic conditions, such as late endosomes and lysosomes. Thus, late endosomes and lysosomes were differentiated using monoclonal antibodies against Rab7 and LAMP1, respectively. These markers of late intracellular pathway after endocytosis were used because of the long incubation time of 24 hours. In K17, fluorescein-labelled SiPs were predominantly associated to LAMP1, confirming their presence in the lysosomes (Figure 5). Some SiPs were also co-localized with Rab7, but to a much lesser extent, suggesting their presence in these organelles, probably right before their transformation into lysosomes. In fact, the particles and LAMP1 were mostly co-localized in the images, indicating that after 24 h of incubation, SiPs have probably been taken up by endocytosis and have entered the classical intracellular degradative pathway, starting in the endosomes toward the lysosomal compartment, where particles can be further degraded.

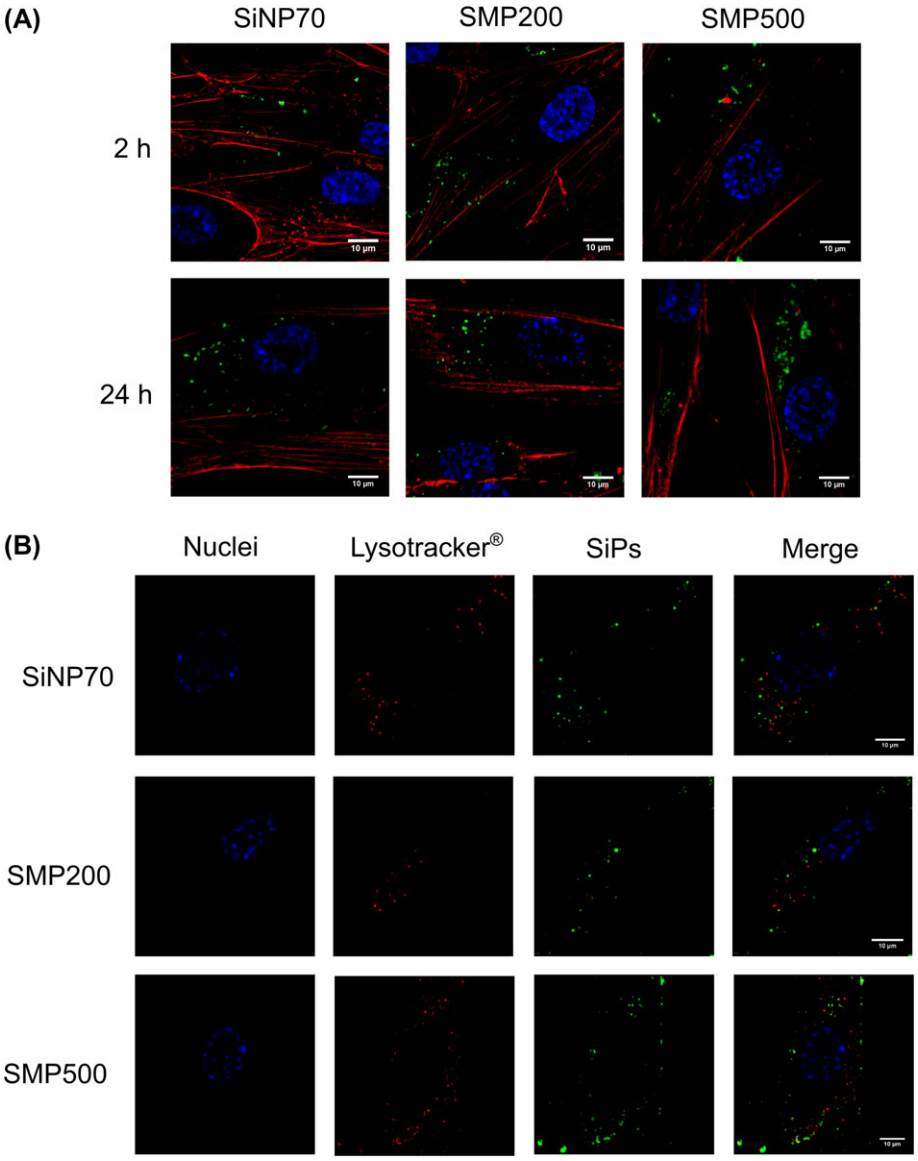

FIGURE 4 LSCM images of fibroblasts incubated with fluorescein-labelled SiNP70, SMP200 and SMP500 at 10 μg/mL. (A) Internalization progress after 2 and 24 h of incubation. Blue channel: Nuclei; green channel: SiPs; red channel: Actin cytoskeleton. (B) Localization of the SiPs in the lysosomal compartment after 24 h of incubation using Lysotracker® as lysosome marker (red channel). Co-localization of SiPs and Lysotracker® are indicated in yellow/orange colour code, as a result of the combination of the green and red channels

In HDF (Figure 6). the co-localization studies with Rab7 and LAMP1 markers indicated that their association with the SiPs did not occur. However, fluorescein-labelled SiPs were always found close to these vesicles, especially late endosomes, and randomly coinciding with the marker signal. These results suggested that silica SiPs might have undergone endosomal escape at the time points studied or the internalization mechanism was not endocytosis. In an additional experiment, SiPs were incubated with HDF for 6 h, and then the protein membrane caveolin-1 was fluorescently labelled. The images showed that SiPs are in close contact with the plasma membrane and concentrate in caveolin-1 rich areas (Figure 7). Indeed, it is possible to observe how caveolin-1-positive signal surrounds and occasionally interacts (co-localization) with SiPs at the cell membrane level, thus confirming this modality of translocation. This endocytosis route is known to bypass lysosomes by the formation of caveosomes with neutral pH (Sahay, Alakhova, & Kabanov, 2010). That would explain the fact that fluorescein-labelled SiPs were intensely internalized but minimally found associated with Rab7 or LAMP1 positive intracellular vesicles.

4 | DISCUSSION

As part of *in vivo* and *in vitro* biological studies involving nanomaterials, particle size distribution, as well as their aggregation/agglomeration state under physiological conditions, are fundamental parameters to be determined (Nichols et al., 2002; Orts-Gil et al., 2010). In fact, the different components of the media always alters the physicochemical properties of the nanomaterials, which could ultimately affect their biological behaviour (Allouni, Cimpan, Hølb, Skodvin, & Gjerdet, 2009).

This study evidenced different effects depending on culture media and original particle size of the materials (Table 2): (a) an increase in average particle size (>1.5 fold increase) and PdI of SiNP20 in both

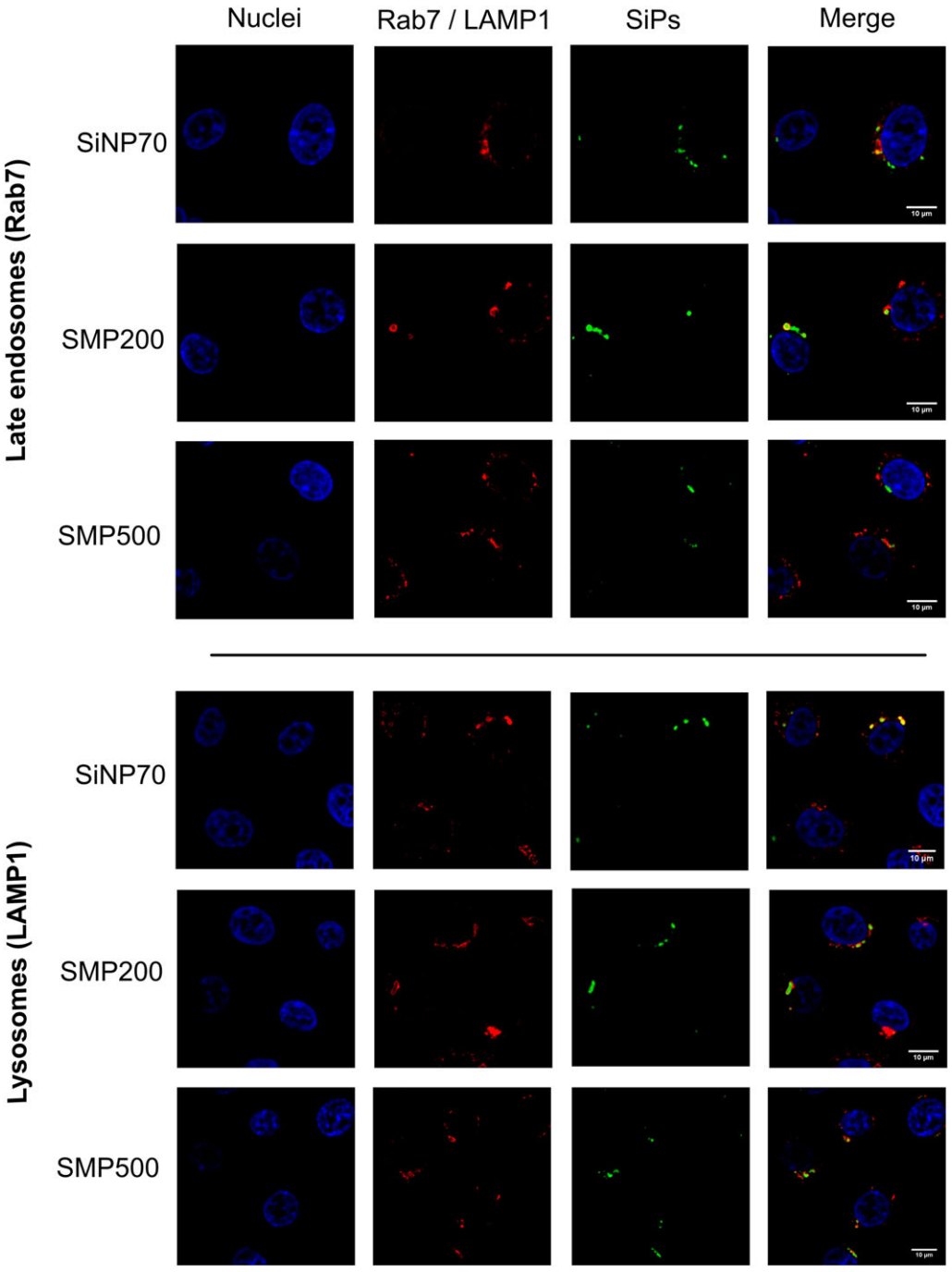

FIGURE 5 LSCM images of keratinocytes incubated with fluorescein-labelled SiNP70, SMP200 and SMP500 at 10 µg/mL. Images were acquired after 24 h of incubation and specifically labelled for Rab7 and LAMP1 to visualize the late endosomes (upper panel) or lysosomes (lower panel), respectively. Co-localization of SiPs and Rab7 or LAMP1 are indicated in yellow/orange color code, as a result of the combination of the green and red channels

media and SiNP70 in EpiLife®; (b) a slight increase in average particle size (<1.5 fold increase) of SiNP70 in Medium 106, SMP200 and SMP500 in EpiLife®; (c) a decrease in average particle size and increase in PdI (>0.3) of SMP200 and SMP500 in Medium 106.

Until recently, the main reason for the colloidal instability of nanoparticles has been assumed to be the high ionic strength of cell culture media, capable of reducing particles' surface potentials (Mukherjee & Weaver, 2010). Indeed, the high content in salts in both media suggests that this parameter can play an important role in the stability of SiPs. For instance, EpiLife® medium contains magnesium chloride ($MgCl_2$ x $6H_2O$), potassium chloride (KCl), and sodium phosphate dibasic (Na_2HPO_4 x $7H_2O$), not present in Medium 106. Such differences can have a direct influence on the ionic strength of the medium, thus affecting particle behaviour once dispersed. Hence, the differences in terms of salts content in both media can be the cause of the formation of sediments for some SiPs (SiNP20 and SiNP70 in EpiLife®, and SMP200 and SMP500 in Medium 106). In addition, recent investigations have determined that when nanomaterials enter a biological fluid, proteins and other biomolecules rapidly compete for binding to its surface, leading to a formation of a dynamic protein layer called protein

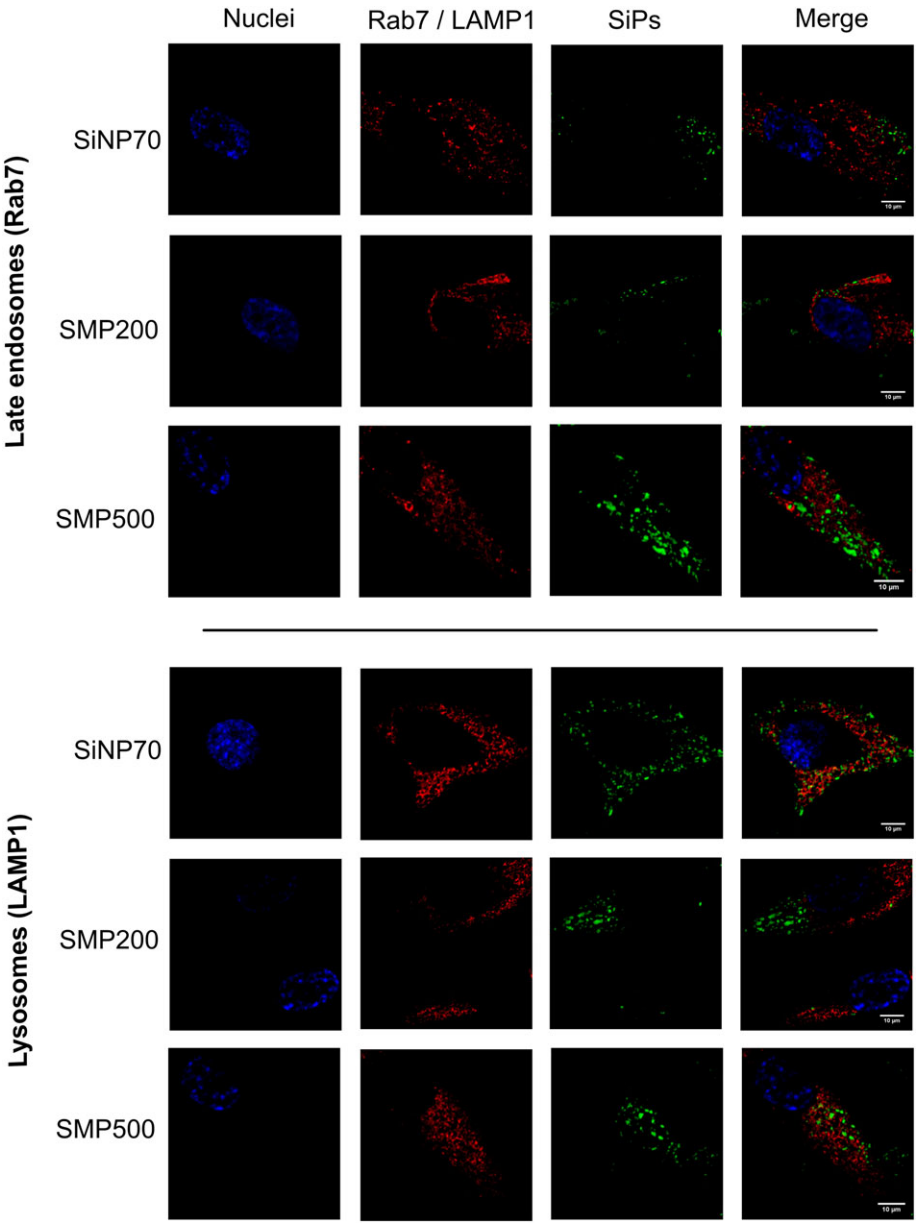

FIGURE 6 LSCM images of fibroblasts incubated with fluorescein-labelled SiNP70, SMP200 and SMP500 at 10 μg/mL. Images were acquired after 24 h of incubation and specifically labelled for Rab7 and LAMP1 in order to visualize the late endosomes (upper panel) or lysosomes (lower panel), respectively. Co-localization of SiPs and Rab7 or LAMP1 are indicated in yellow/orange color code, as a result of the combination of the green and red channels

corona (PC). In fact, the slight particle size increase without sedimentation (situation (b)) could be attributed to the formation of this stable protein corona around the particles. Nevertheless, protein adsorption could also be a source of colloidal instability that might contribute to agglomeration or aggregation (Orts-Gil et al., 2010), as occurred in (a). One major factor influencing protein adsorption is particle size, with smaller particles having more tendency to aggregate. It has been observed that less ordered and more denatured proteins bound to smaller nanoparticles can lead to particle aggregation (Roach, Farrar, & Perry, 2006). It is also possible that proteins form 'bridges' between particles that increase their tendency to agglomerate (Orts-Gil et al., 2013). Protein composition of the media EpiLife® and 106 is also very different. Therefore, the components of the PC could differ, thus leading to these different behaviours.

Studies using *in vitro* and *in vivo* models to delineate size-dependent toxicological effects of SiPs have been increasingly documented (Brown, Kanase, Gaiser, Johnston, & Stone, 2014; Docter et al., 2014). This present study demonstrated that nanoparticles (SiPs <200 nm) induced higher rates of cell death in a concentration- and size-dependent manner. In particular, nanoparticles with the smallest size (SiNP20) were strong inducers of apoptosis at low concentrations, evidencing intracellular damage. In addition, the size increment from 20 to 70 nm importantly increased the viability levels, being more similar to those achieved by sub-microparticles (SiPs ≥200 nm). These results are in agreement with previous findings describing that cytotoxicity generated by SiPs strongly depended on particle size and administered dose, with smaller silica particles producing a higher toxic effect (Guichard et al., 2016). Similar results were observed by

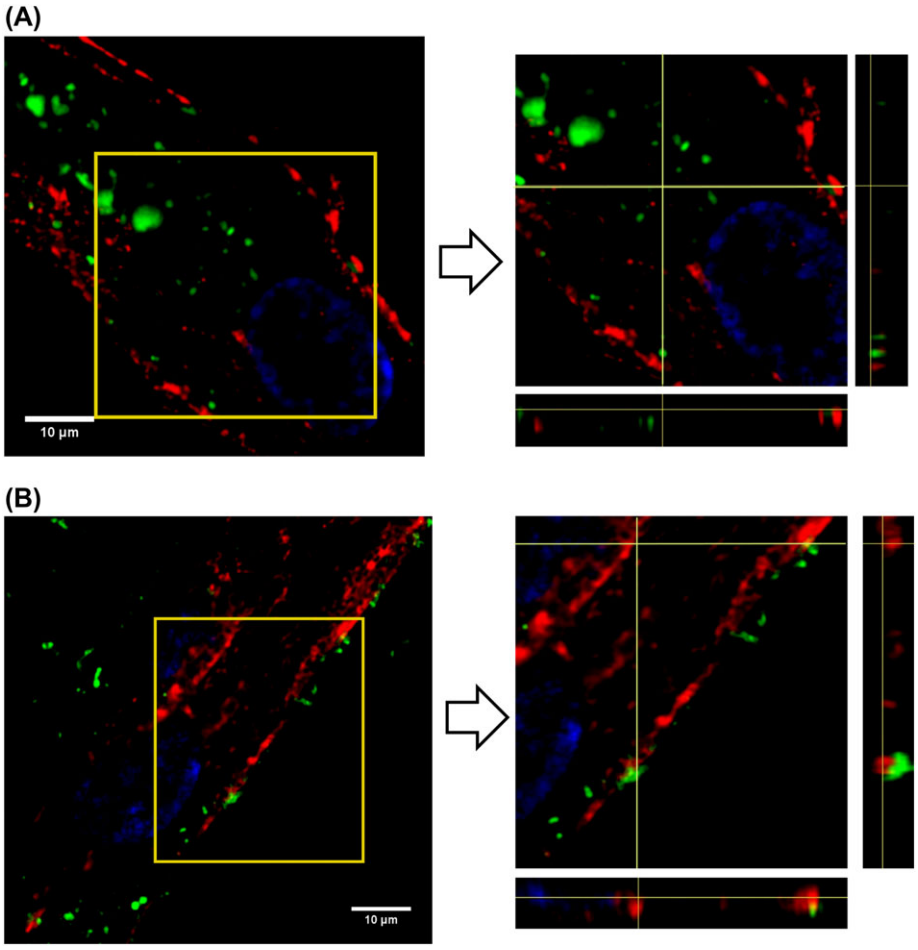

FIGURE 7 LSCM images of fibroblasts incubated with fluorescein-labelled SiNP 70 (representing silica nanoparticles) (A) and SMP200 (representing silica sub-microparticles) (B) at 10 µg/mL. Images were acquired after 6 h of incubation and specifically labelled for caveolin-1. The right panel offers a detailed view of the image of the left with the orthogonal views XZ and YZ. Blue channel: Nuclei; green channel: SiPs; red channel: Caveolin-1

McCarthy, Inkielewicz-Stepniak, Corbalan, and Radomski (2012) using 10, 150 and 500 nm SiPs in Calu-3 cells. In line with our data, the authors also observed that the particles of 150 and 500 nm did not induce cytotoxicity after 24 h of incubation. A study comparing 15 and 55 nm silica nanoparticles in the Caco-2 cell line (Tarantini et al., 2015) showed that the smallest particles induced higher rates of cell death. This high toxicity has been attributed to an increased induction of reactive oxygen species (ROS) together with an inflammatory response mediated by IL-8. The increased surface area and a number of particles added per dose of ultra-small nanoparticles compared to larger particles were claimed to be the main cause of this adverse response. Altogether, these findings lead to the general conclusion that there exist a size-dependency of SiPs affecting cytotoxicity. However, it is important to note that although most of the studies indicate that small nanoparticles are more toxic than their larger counterparts, the size dependent mode of action is still elusive and other factors, such as external coating, chemical modifications, cell lines used, etc., can modify this trend. In fact, SiNP70, SMP200 and SMP500 showed little to no toxicological effect in a wide range of concentrations without evidencing a clear particle size effect. This could be due to the formation of the external PC, which modifies their physicochemical properties. Indeed, the formation of this PC has been gaining relevance because it can affect the interaction of nanomaterials with the biological environment (Faroozah & Aziz, 2015), as cells interact with the entire nanoparticle–protein corona complexes rather than with the bare nanoparticle (Lynch & Dawson, 2008; Lynch et al., 2007).

Furthermore, it is noteworthy to remark the relevance of the cell type used when analysing cytotoxicity of SiPs (Kim, Joachim, Choi, & Kim, 2015). In our observations, K17 were more affected by the treatment with SiPs, which was especially evident on the LDH and apoptosis assays (Figure 2). This increased sensitivity of keratinocytes vs. fibroblasts has been previously described by Olschläger, Schrader, and Hockertz (2009). This study established different sensitivities to a toxin according to the cell type, being primary keratinocytes more sensitive than primary fibroblasts. Growth and differentiation factors have also been described to influence cellular sensitivity to external treatments, being low differentiation and slow growth determinant for lower sensitivity and vice versa (Hsiao et al., 2012; Kolbe et al., 2011; Singh et al., 2014; Wiegand & Hipler, 2008). Translating this to the present study, keratinocytes are characterized by rapid growth and differentiation, whereas fibroblasts grow slower and do not undergo morphological differentiation.

In general, it has been considered that high cellular uptake rates of nanoparticles lead to strong toxic response due to the accumulation inside the cell, affecting its normal functions. SiPs studied here were intensely internalized regardless their original particle size. The

internalization kinetics depended mostly on the cell type, being faster for K17 than for HDF, although after 24 hours of incubation SiPs were taken up in large amounts in both cell types. This difference in the kinetics could be due to a different internalization process. While keratinocytes are more prone to phagocytosis of extracellular materials (Lopes et al., 2016), fibroblasts do not show a so defined uptaking profile (Zhang, Hu, Yu, & Gao, 2010). In fact, in K17, SiPs were found engulfed in lysosomes after 24 h, whereas in HDF no clear association with lysosomes or endosomes was observed. Therefore, it can be deduced that the strong affinity of the SiPs for the plasma membrane of K17 could have induced the rapid initiation of phagocytosis of the particles adsorbed to the membrane and subsequently translocate towards the intracellular degradation pathway (Hillareau & Couvreur, 2009). Further imaging has led us to the conclusion that the main internalization mechanism in HDF could be mediated by caveolae. This endocytosis modality has been described to be slower than other internalization mechanisms and characterized by the formation of neutral vesicles (caveosomes), hence undetectable by Lysotracker® (Sahay et al., 2010). Therefore, the close interaction of SiPs with caveolin-1 on the plasma membrane (Figure 7) and the low association with lysosomes (Figure 4B) would support this hypothesis. However, there could co-exist different endocytosis mechanisms in the internalization of SiPs in dermal fibroblasts that would need to be further explored (Zhang, Hu, Yu, & Gao, 2010). In addition, the different intracellular location of SiPs in either K17 or HDF might also explain the different resistance to SiPs exposure of both cell types. Recently published research by Wang et al. (2017) hypothesized that the accumulation of SiPs in lysosomes could be the cause of the higher toxicity rate observed in K17 related to HDF. Authors determined that SiPs in lysosomes can impair their function causing autophagy dysfunction. This dysfunction can further result in a blockage of normal autophagy degradation route thus, accumulating intracellular disposal materials inside the cell and in consequence increase apoptosis/cell death. Since, SiPs do not accumulate in lysosomes of HDF, these cells would not suffer this anomaly, thus increasing their tolerance to SiPs exposure.

Altogether, the toxicological data obtained for SiPs in K17 and HDF suggest that SiNP20 are not suitable as drug delivery carriers for the skin. In contrast, particles larger than 70 nm demonstrated to be non-toxic for both dermal cells in a wide range of concentrations.

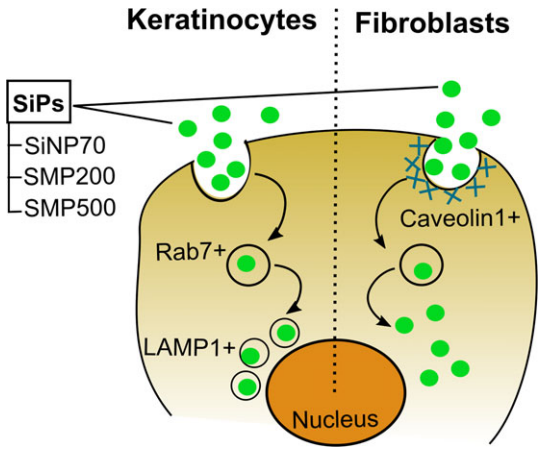

FIGURE 8 Schematic overview of the different internalization routes of SiPs in both keratinocytes and fibroblasts

The internalization studies indicated that the particles fate inside the cells was strongly cell-type dependent (Figure 8). Consequently, when using SiPs for skin drug delivery, it is crucial to define the targeted cell type. For instance, they can be an interesting platform for delivering pro-drugs to keratinocytes due to the facilitated uptake and intracellular transport towards the lysosome, which ultimately would accelerate drug release. In contrast, fibroblasts would be the targets of SiPs for delivering more delicate molecules such as proteins or genetic material to be preserved from rapid degradative processes. In addition, the versatility of these SiPs enable their surface modification to avoid or take advantage of their intracellular fate while maintaining their low cytotoxicity profile.

ACKNOWLEDGEMENTS

This work was supported by the European Commission: FP7 People Marie Curie Actions, project NANODRUG [MCITN-2011-289554]. S. Vicente acknowledges the Marie Curie Industry Host Fellowship [HPMI-CT-2001-00110]. We would like to thank Prof. David Kelsell and Dr. Benjamin Fell (Queen Mary University of London, UK) for providing K17 keratinocytes and their valuable advice regarding K17 culture.

CONFLICT OF INTEREST

S. Vicente and X. Vigé were employees of Sanofi Research & Development, Chilly-Mazarin, France; during the execution of this study. The other authors declare no competing financial interest.

REFERENCES

Alex, S. M., & Sharma, C. P. (2013). Nanomedicine for gene therapy. *Drug Delivery and Translational Research*, *3*(5), 437–445.

Allouni, Z. E., Cimpan, M. R., Hølb, P. J., Skodvin, T., & Gjerdet, N. R. (2009). Agglomeration and sedimentation of TiO_2 nanoparticles in cell culture medium. *Colloids and Surfaces. B, Biointerfaces*, *68*, 83–87.

Arora, S., Rajwade, J. M., & Paknikar, K. M. (2012). Nanotoxicology and *in vitro* studies: The need of the hour. *Toxicology and Applied Pharmacology*, *258*, 151–165.

Bakhtiary, Z., Saei, A. A., Hajipour, M. J., Raoufi, M., Vermesh, O., & Mahmoudi, M. (2016). Targeted superparamagnetic iron oxide nanoparticles for early detection of cancer: Possibilities and challenges. *Nanomedicine*, *12*(2), 287–307.

Brown, D. M., Kanase, N., Gaiser, B., Johnston, H., & Stone, V. (2014). Inflammation and gene expression in the rat lung after instillation of silica nanoparticles: Effect of size, dispersion medium and particle surface charge. *Toxicology Letters*, *224*(1), 147–156.

Caster, J. M., Pate, A. N., Zhang, T., & Wang, A. (2017). Investigational nanomedicines in 2016: A review of nanotherapeutics currently undergoing clinical trials. *Wiley Interdisciplinary Reviews. Nanomedicine and Nanobiotechnology*, *9*(1). e1416

Correia-Pinto, J. F., Csaba, N., & Alonso, M. J. (2013). Vaccine delivery carriers: Insights and future perspectives. *International Journal of Pharmaceutics*, *440*(1), 27–38.

Docter, D., Bantz, C., Westmeier, D., Galla, H. J., Wang, Q., Kirkpatrick, J. C., … Stauber, R. H. (2014). The protein corona protects against size and dose-dependent toxicity of amorphous silica nanoparticles. *Beilstein Journal of Nanotechnology*, *5*, 1380–1392.

Duncan, R., & Gaspar, R. (2011). Nanomedicine(s) under the microscope. *Molecular Pharmaceutics*, *8*(6), 2101–2141.

Faroozah, P., & Aziz, A. A. (2015). Merging worlds of nanomaterials and biological environment: Factors governing protein corona formation on nanoparticles and its biological consequences. *Nanoscale Research Letters*, *10*, 221.

Fruitjier-Pölloth, C. (2012). The toxicological mode of action and the safety of synthetic amorphous silica – A nanostructured material. *Toxicology*, *294*, 61–79.

Guichard, Y., Fontana, C., Chavinier, E., Terzetti, F., Gaté, L., Binet, S., & Darne, C. (2016). Cytotoxic and genotoxic evaluation of different synthetic amorphous silica nanomaterials in the V79 cell line. *Toxicology and Industrial Health*, *32*(9), 1639–1650.

Hillareau, H., & Couvreur, P. (2009). Nanocarriers' entry into the cell: relevance to drug delivery. *Cellular and Molecular Life Sciences*, *66*, 2873–2896.

Hsiao, S. T., Asgari, A., Lokmic, Z., Sinclair, R., Dusting, G. J., Lim, S. Y., & Dilley, R. J. (2012). Comparative analysis of paracrine factor expression in human adult mesenchymal stem cells derived from bone marrow, adipose, and dermal tissue. *Stem Cells and Development*, *21*(12), 2189–2203.

Iannuccelli, V., Bertelli, D., Romagnoli, M., Scalia, S., Maretti, E., Sacchetti, F., & Leo, E. (2014). *In vivo* penetration of bare and lipid-coated silica nanoparticles across the human *stratum corneum*. *Colloids and Surfaces. B, Biointerfaces*, *122*, 653–661.

Kettiger, H., Karaman, D. S., Schiesser, L., Rosenholm, R. M., & Höwyler, J. (2015). Comparative safety evaluation of silica-based particles. *Toxicology In Vitro*, *30*(1B), 355–363.

Kim, I. Y., Joachim, E., Choi, H., & Kim, K. (2015). Toxicity of silica nanoparticles depends on size, dose, and cell type. *Nanomedicine*, *11*(6), 1407–1416.

Kolbe, M., Xiang, Z., Dohle, E., Tonak, M., Kirkpatrick, C. J., & Fuchs, S. (2011). Paracrine effects influenced by cell culture medium and consequences on microvessel-like structures in co-cultures of mesenchymal stem cells and outgrowth endothelial cells. *Tissue Engineering. Part A*, *17-18*, 2199–2212.

Krishnamurty, S., Ke, X., & Yang, Y. Y. (2015). Delivery of therapeutics using nanocarriers for targeting cancer cells and cancer stem cells. *Nanomedicine (Lond)*, *10*(1), 143–160.

Liberman, A., Mendez, N., Trogler, W. C., & Kummel, A. C. (2014). Synthesis and surface functionalization of silica nanoparticles for nanomedicine. *Surface Science Reports*, *69*, 132–158.

Lopes, V. R., Loitto, V., Audinot, J. N., Bayat, N., Gutleb, A. C., & Cristobal, S. (2016). Dose-dependent autophagic effect of titanium dioxide nanoparticles in human HaCaT cells at non-cytotoxic levels. *Journal of Nanbiotechnology*, *14*, 22.

Lynch, I., Cedervall, T., Lundqvist, M., Cabaleiro-Lago, C., Linse, S., & Dawson, K. A. (2007). The nanoparticle–protein complex as a biological entity; a complex fluids and surface science challenge for the 21st century. *Advances in Colloid and Interface Science*, *134-135*, 167–174.

Lynch, I., & Dawson, K. A. (2008). Protein-nanoparticle interactions. *Nano Today*, *3*, 40–47.

McCarthy, J., Inkielewicz-Stepniak, I., Corbalan, J. J., & Radomski, M. W. (2012). Mechanisms of toxicity of amorphous silica nanoparticles on human lung submucosal cells *in vitro*: Protective effects of fisetin. *Chemical Research in Toxicology*, *25*(10), 2227–2235.

Mukherjee, B., & Weaver, J. W. (2010). Aggregation and charge behavior of metallic and nonmetallic nanoparticles in the presence of competing similarly-charged inorganic ions. *Environmental Science & Technology*, *44*, 3332–3338.

Muthu, M. S., Leong, D. T., Mei, L., & Feng, S. S. (2014). Nanotheranostics: Application and further development of nanomedicine strategies for advanced theranostics. *Theranostics*, *4*(6), 660–677.

Nafisi, S., Schäfer-Korting, M., & Maibach, H. I. (2015). Perspectives on percutaneous penetration: Silica nanoparticles. *Nanotoxicology*, *9*(5), 643–657.

Napierska, D., Thomassen, L. C. J., Lison, D., Martens, J. A., & Hoet, P. H. (2010). The nanosilica hazard: Another variable entity. *Particle and Fibre Toxicology*, *7*, 39.

Nichols, G., Byard, S., Bloxham, M. J., Botterill, J., Dawson, N. J., Dennis, A., … Sherwood, J. D. (2002). A review of the terms agglomerate and aggregate with a recommendation for nomenclature used in powder and particle characterization. *Journal of Pharmaceutical Sciences*, *91*(10), 2103–2109.

Olschläger, V., Schrader, A., & Hockertz, S. (2009). Comparison of primary human fibroblasts and keratinocytes with immortalized cell lines regarding their sensitivity to sodium dodecyl sulfate in a neutral red uptake cytotoxicity assay. *Arzneimittel-Forschung*, *59*(3), 146–152.

Orts-Gil, G., Natte, K., Drescher, D., Bresch, H., Mantion, A., Kneipp, J., & Österle, W. (2010). Characterisation of silica nanoparticles prior to *in vitro* studies: From primary particles to agglomerates. *Journal of Nanoparticle Research*, *13*, 9910.

Orts-Gil, G., Natte, K., Thiermann, R., Girod, M., Rades, S., Kalbe, H., … Österle, W. (2013). On the role of surface composition and curvature on biointerface formation and colloidal stability of nanoparticles in a protein-rich model system. *Colloids and Surfaces. B, Biointerfaces*, *108*, 110–119.

Ponnappan, N., & Chugh, A. (2015). Nanoparticle-mediated delivery of therapeutic drugs. *Pharmaceutical Medicine*, *29*(3), 155–167.

Roach, P., Farrar, D., & Perry, C. C. (2006). Surface tailoring for controlled protein adsorption: Effect of topography at the nanometer scale and chemistry. *Journal of the American Chemical Society*, *128*, 3939–3945.

Sahay, G., Alakhova, D. Y., & Kabanov, A. V. (2010). Endocytosis of nanomedicines. *Journal of Controlled Release*, *145*(3), 182–195.

Santamaria, A. (2012). Historical overview of nanotechnology and nanotoxicology. In J. Reineke (Ed.), *Nanotoxicity* (pp. 1–12). New York: Humana Press.

Singh, D., Singh, D., Choi, S. M., Zo, S., Painuli, R. M., Kwon, S. W., & Han, S. S. (2014). Effect of extracts of *Terminalia chebula* on proliferation of keratinocytes and fibroblasts cells: An alternative approach for wound healing. *Evidence-based Complementary and Alternative Medicine*, *2014*. ID701656

Tarantini, A., Lanceleur, R., Mourot, A., Lavault, M. T., Casterou, G., Jarry, G., … Fessard, V. (2015). Toxicity, genotoxicity and proinflammatory effects of amorphous nanosilica in the human intestinal Caco-2. *Toxicology In Vitro*, *29*(2), 398–407.

Ugazio, E., Gastald, L., Brunella, V., Scalarona, D., Jadhav, S. A., Oliaro-Bosso, A., … Sapino, S. (2016). Thermoresponsive mesoporous silica nanoaparticles as carrier for skin delivery of quercetin. *International Journal of Pharmaceutics*, *511*(1), 446–454.

Wang, J., Yu, Y., Lu, K., Yang, M., Li, Y., Zhou, X., & Sun, Z. (2017). Silica nanoparticles induce autophagy dysfunction via lysosomal impairment and inhibition of autophagosome degradation in hepatocytes. *International Journal of Nanomedicine*, *12*, 809–825.

Wiegand, C., & Hipler, U. (2008). Methods for the measurement of cell and tissue compatibility including tissue regeneration processes. *GMS Krankenhhyg Interdiszip*, *3*(1). Doc12

Yu, K. O., Grabinski, C. M., Schrand, A. M., Murdock, R. C., Wang, W., Gu, B., … Houssain, S. M. (2009). Toxicity of amorphous silica nanoparticles in mouse keratinocytes. *Journal of Nanoparticle Research*, *11*(1), 15–24.

Zhang, Y., Hu, L., Yu, D., & Gao, C. (2010). Influence of silica particle internalization on adhesion and migration of human dermal fibroblasts. *Biomaterials*, *31*, 8465–8474.

SUPPORTING INFORMATION

Additional Supporting Information may be found online in the supporting information tab for this article.

How to cite this article: Vicente S, Moia C, Zhu H, Vigé X. *In vitro* evaluation of the internalization and toxicological profile of silica nanoparticles and submicroparticles for the design of dermal drug delivery strategies. *J Appl Toxicol*. 2017;37: 1396–1407. https://doi.org/10.1002/jat.3507